

Research Article

Biodegradation of poly(ethylene terephthalate) through PETase surface-display: From function to structure



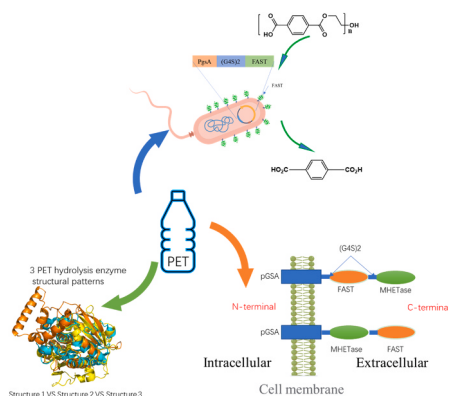
Wei Han, Jun Zhang, Qi Chen, Yuzhu Xie, Meng Zhang, Jianhua Qu, Yuanji Tan, Yiran Diao, Yixuan Wang, Ying Zhang*

School of Resources and Environment, Northeast Agricultural University, Heilongjiang 150030, PR China

HIGHLIGHTS

- In the PETase surface display, the anchoring protein types had little effect on the results.
- Surface-display of FAST-PETase has shown great potential for PET hydrolysis.
- There are three main crystal structure patterns of PET hydrolysis enzyme, with ISPETase being the representative enzyme.
- The size and crystallinity of the PET particles play a crucial role in the hydrolysis efficiency of PET.
- The surface co-display sequential of FAST-PETase and MHETase has effect on PET hydrolysis.

GRAPHICAL ABSTRACT



ARTICLE INFO

Editor: Lingxin CHEN

Keywords:

Poly(ethylene terephthalate)
PETase
Surface-display
Crystal structure

ABSTRACT

Polyethylene terephthalate (PET) is one of the most used plastics which has caused some environmental pollution and social problems. Although many newly discovered or modified PET hydrolases have been reported at present, there is still a lack of comparison between their hydrolytic capacities, as well as the need for new biotechnology to apply them for the PET treatment. Here, we systematically studied the surface-display technology for PET hydrolysis using several PET hydrolases. It is found that anchoring protein types had little influence on the surface-display result under T7 promoter, while the PET hydrolase types were more important. By contrast, the newly reported FAST-PETase showed the strongest hydrolysis effect, achieving 71.3% PET hydrolysis in 24 h by pGSA-FAST-PETase. Via model calculation, FAST-PETase indeed exhibited higher temperature tolerance and catalytic capacity. Besides, smaller particle size and lower crystallinity favored the hydrolysis of PET pellets. Through protein structure comparison, we summarized the common characteristics of efficient PET-hydrolyzing enzymes and proposed three main crystal structures of PET enzymes via crystal structural analysis, with ISPETase being the representative and main structure. Surface co-display of FAST-PETase and MHETase can promote the hydrolysis of PET, and the C-terminal of the fusion protein is crucial for PET hydrolysis. The results of our research can be helpful for PET contamination removal as well as other areas involving the application of enzymes.

* Corresponding author.

E-mail address: zhangying_neau@163.com (Y. Zhang).

Synopsis: This research can promote the development of better PET hydrolase and its applications in PET pollution treatment via bacteria surface-display.

1. Introduction

Owing to the robustness, impermeability to gases and high transparency, polyethylene terephthalate (PET) has emerged as a prevailing material in the packaging and textile industry[1]. According to statistics, its global annual production capacity reached 30.5 million tons in 2019 and is expected to increase to 35.3 million tons by 2024[2]. Currently, plastic fragments and particles, including microplastics and nanoplastics, have been found in marine environments and various species, highlighting the urgent need for comprehensive actions to resolve this prevalent issue[3,4]. Over the last decade, many enzymes originating from microbes have been identified as capable of cleaving the ester bond linkages in PET, including esterases, PETase (EC 3.1.1.101), carboxylesterases, and cutinases (EC 3.1.1.74) [5]. Among them, the most renowned one is *Ideonella Sakaiensis* 201-F6, first reported in 2016 for its exceptional ability to efficiently depolymerize PET films[6]. By conducting a detailed analysis of both protein and gene sequences, the authors identified two key enzymes, namely *IsPETase* and *MHETase*, which formed the core of efficient PET depolymerization process. With the discovery of *IsPETase*, a large number of natural PET hydrolase were discovered successively from isolated bacteria and shotgun metagenome sequence assembling[7]. However, considering the thermal instability of natural *IsPETase* enzymes and high glass transition temperature of PET, some PETase mutants were published with enhanced hydrolysis activity and stability compared to the wild type[8,9]. Despite the promising results in the discovery of PET hydrolases, their practical engineering applications have not been thoroughly evaluated or compared.

Cell surface-display is an innovative technique that can anchor a target protein to the outer membrane of a cell, which facilitates the preservation of enzyme function and activity, and enhances the stability and reusability of enzyme in the cell surface[10]. Compared with intracellular expression and secretion, cell surface-display technology has unique advantages: 1) Enzyme displayed on the cell outer membrane can maintain function under harsh conditions. 2) Enzyme displayed can play the role directly, avoiding the complex process of lysing cells or protein purification. 3) Co-display of multi-enzyme enzymes can improve catalytic efficiency. 4) Surface-displayed functional enzymes can act on large molecular mass substrates[11]. Although some attempts on PET hydrolase surface-display have been reported with a certain results[12–14], there is still a lack of researches on the selection of anchoring proteins, the comparison of different PET hydrolases, and a series of issues arising from them, especially the hidden mechanisms involved.

In this work, we conducted a systematic study on how to construct surface-displayed engineered bacteria for the hydrolytic treatment of PET plastics. In order to study the effect of anchoring protein types on the surface-display system, three different anchoring proteins were selected for the construction, including *inaXN*, *estA*, *pGSA*. At the same time, four PET hydrolases were chosen for the degradation of PET plastics, including three newly reported enzymes and the most well-known *IsPETase*. Among the surface-display systems built, *pGSA*-FAST-PETase exhibited the highest PET hydrolytic performance at 50 °C. In addition, we investigated the effect of ion addition, particle size and crystallinity of PET particle on PET degradation via *pGSA*-FAST-PETase engineered bacteria. In order to investigate the intrinsic reasons of hydrolysis differences, crystal structure analysis and molecular dynamics simulation were introduced for the study. Notably, the co-display of *MHETase* and FAST-PETase exhibited enhanced PET hydrolysis result, and the hydrolysis capacity and products varied as the

change of the enzyme in fusion protein C-terminal end. Our results not only deepen the understanding of PET hydrolases, but also can provide some theoretical guidance in facing other enzymes for surface-display applications. Importantly, the application of comparative protein structure analyses and molecular dynamics simulations can facilitate the systematic investigation and comparison of PET hydrolases.

2. Materials and methods

2.1. Materials and methods

2.1.1. Culture conditions and plasmid construction

The gene sequences utilized in this investigation are specified in the Supporting Information (SI) Table 1. The PET-30a vector backbone was employed for plasmid construction in this study, and *E. coli* DH5α was used for cultivated in LB medium (1% w/v tryptone, 0.5% w/v yeast extract, and 1% w/v NaCl) with 50 µg/mL kanamycin at 37 °C. PET-30 vector backbone is a commonly used vector, possessing the T7 promoter, which can accomplish a large amount of the target protein expression in a short period of time. And this vector possesses more enzyme cleavage sites, which can facilitate the recombination of anchored proteins and multiple enzymes. The anchor proteins sequences were downloaded from NCBI, including *pGSA*[15] (poly-γ-glutamate synthetase A protein, ACT52837.1), *inaXN*[16] (ice nucleation protein N-domain, ACN91081.1), and *estA*[17] (outer membrane esterase autotransporter, CP034908). All expression vectors were transformed into BL21(DE3) through heat shock (37 °C), and the detailed procedural steps can be found in a prior study[12]. To induce the surface-display protein expression, 0.1 mM isopropyl-D-1-thiogalactopyranoside (IPTG) was added to the culture ($OD_{600}=0.7$) under shaking conditions at 20 °C for 16 h. And all the plasmid maps were supplied in Supplementary Information and the sequences used were shown in SI Table S1. To remove interference from the culture medium, all bacteria were used by centrifugation, washed three times by PBS, and resuspended in PBS ($OD_{600}=1$).

2.2. Enzyme activity assay and weight loss for PET

A total of 80 µL phosphate-buffered saline (PBS) buffer, 10 µL p-nitrophenyl butyrate (pNPB, 8 mM)[14], and 10 µL bacterial solution ($OD_{600}=1$) were successively added into a 2 mL centrifuge tube to react for 5 min. After the reaction was completed, 100 µL ethanol was added to halt the reaction, and subsequently cooled to room temperature on ice. The reaction product was then transferred into a 96-well plate for quantification and the formation of p-nitrophenol was recorded at a wavelength of 405 nm. As a negative control, BL21(DE3) cells without any surface-display expression vectors were utilized.

PET film (0.1 mm thick) and PET powder with different particles (50, 200, 500, 1000, 2000 mesh) are purchased from the market (roll or granular material). 4 g PET powder or 3 pieces 1 cm × 1 cm films were placed in a 250 mL conical flask. Next, 100 mL bacterial solution ($OD_{600}=1$) was added, and the flask was sealed with a membrane. The mixture was positioned on a constant temperature shaker at 180 rpm for 24 h before being terminated on ice. Then, the PET materials were filtered, and rinsed with ultrapure water, 0.1% SDS and ethanol, successively. After dried thoroughly at room temperature for 48 h, the weight of PET particles was measured and recorded.

2.3. Double-chambered experiment

This experiment involved separating the whole-cell catalytic bacteria and PET plastics using a semi-permeable membrane. 250 mL bacterial solution was loaded into the left chamber of the reactor. A certain amount of PET plastic films and particles was measured and placed in the right chamber with same amount of PBS. The assembled instrument was placed on a water bath shaker at 50 °C for 24 h. The experimental setup of the double-chambered experiment is depicted in the SI Fig. S9.

2.4. Enzyme-linked immunomagnetic bead precipitation

20 µL Anti-His magnetic beads were gently mixed by pipetting and added to a clean centrifuge tube with 480 µL 1X TBS to reach a final volume of approximately 0.5 mL. Then the Anti-His magnetic beads mixture was mixed with bacterial solution and placed on a magnetic rack for 10 s to separate. Finally, the OD₆₀₀ of the supernatant was measured.

2.5. Bacterial outer membrane protein extraction

The Membrane Protein Extraction Kit (Sangon Biotech, China) was used to extract the outer membrane proteins from *E. coli* BL21. The detailed process can be referred to the manual.

2.6. Effect of temperature, pH, metal ions on hydrolase activity of PET

The enzymatic activity at different temperatures was measured using pNPB as the substrate, with the maximum enzymatic activity defined as 100%. For the effect of metal ions, the enzymatic activity was measured after incubation at 50 °C for 24 h in the presence of NaCl, KCl, CuCl₂, MgCl₂, CaCl₂, and Fe₃Cl₃ with a final concentration of 10 mM in the system. And pH experiment was performed by the same method.

2.7. Hydrolysis ability of PET powders with different particle sizes

250 mL induced bacterial liquid (OD₆₀₀ = 1) was taken and adjusted to pH = 8.5. Different sizes of PET powder (50, 200, 500, 1000, and 2000 mesh) were separately weighed and added, then hydrolyzed at 50 °C for 24 h. This process was repeated three times and calculate the final weight loss rate.

2.8. Hydrolysis ability of PET powders with different PET bottle crystallinity

The PET plastic bottle with the “01” symbol at the bottom was divided into three parts, including the bottle cap, body, and bottom. Each part was ground using a grinder and collected through a 200-mesh sieve. The collected powders were added separately to the bacterial

Table 1

Protein crystal structure alignment result (TM-score: normalized by average length of two structures).

Structure class	Category	PDB ID	Strain	Year	TM-score	RMSD
Structure 1	ISPETase	5XG0	<i>Ideonella sakaiensis</i> 201-F6	2017		
		5XJH	<i>Ideonella sakaiensis</i>	2018	0.988	0.5
		5YFE	<i>Ideonella sakaiensis</i>	2018	0.984	0.57
		6ANE	<i>Ideonella sakaiensis</i>	2018	0.996	0.25
		6EQD,6EQE,6EQH	<i>Ideonella sakaiensis</i>	2018	0.994	0.28
		6AID	<i>Thermobifida alba</i>	2019	0.938	1.28
		7CWQ	<i>Burkholderiales bacterium</i>	2021	0.966	0.87
		7QJO	<i>Marinactinospora thermotolerans</i> DSM45154	2022	0.931	1.33
		7QJP	<i>Saccharopolyspora flava</i>	2022	0.931	1.26
		7QJQ	<i>Thermobifida fusca</i> NTU22	2022	0.94	1.3
	Cutinase	7QJR	<i>Thermobifida fusca</i> DSM44342	2022	0.935	1.3
		7QJS	<i>Thermobifida fusca</i> YX	2022	0.94	1.24
		7QJT	<i>Thermobifida cellulosilytica</i>	2022	0.928	1.28
		3VIS(Est119)	<i>Thermobifida alba</i> AHK119	2012	0.941	1.32
		7PZJ	<i>Bacteroidetes Aequorivita</i> sp.	2022	0.887	1.64
		4EB0	Leaf-branch compost bacterial cutinase homolog	2012	0.93	1.36
		6SBN	<i>Pseudomonas aestusnigri</i>	2019	0.928	1.71
		7CUV	metagenome-derived from apo form	2021	0.943	1.14
		7W69	metagenome-derived from apo form	2021	0.945	1.15
		7EOA	marine <i>Bacillus</i> HR29	2021	0.93	1.33
	Esterase	7DZT	<i>Rhizobacter gummiphilus</i>	2021	0.972	0.75
		7NEI	Metagenomic Polyester Hydrolase	2022	0.945	1.13
		7VMD	Ple628 from marine microbial consortium	2022	0.926	1.69
		7VPA	Ple629 from marine microbial consortium	2022	0.945	1.23
		7Z6B	<i>Vibrio gazogenes</i>	2022	0.934	1.29
		8D1D	PROSS PETase	2022	0.992	0.85
		4CG1	<i>Thermobifida Fusca</i>	2013	0.937	1.28
		4CG2	<i>Thermobifida Fusca</i>	2013	0.939	1.28
		4CG3	<i>Thermobifida Fusca</i>	2013	0.935	1.28
		3WYN	<i>Thermobifida alba</i> . cutinase Est119	2014	0.941	1.35
	TfCut	5LUI	<i>Thermobifida cellulosilytica</i> cutinase	2017	0.933	1.28
		5LUJ	<i>Thermobifida cellulosilytica</i> cutinase	2017	0.938	1.23
		5LUK	<i>Thermobifida cellulosilytica</i> cutinase	2017	0.936	1.28
		5LUL	<i>Thermobifida cellulosilytica</i> cutinase	2017	0.938	1.27
		5ZOA	<i>Thermobifida fusca</i> cutinase	2019	0.938	1.31
		7DS7	Biortus	2020	0.931	1.34
		5AJH	<i>Fusarium oxysporum</i>	2015		
		7CY3	<i>Paraphoma</i> sp. B47-9	2020	0.962	0.87
		4OYY	<i>Humicola insolens</i> cutinase	2014	0.95	0.76
		7QJM	<i>Chloroflexus</i> sp. MS-G			
Structure 2	PEH	7QIN	Candidatus <i>Kryptobacter tengchongensis</i>		0.947	0.86
		5XG0 VS 5AJH			0.56	
		5XG0 VS 7QJM			0.654	
		5AJH VS 7QJM			0.541	

solution and hydrolyzed at 50 °C for 24 h, and weight loss rates were calculated at last.

2.9. Molecular dynamics (MD) simulations and molecular docking

Gromacs 2020 is used for the all-atom MD simulations using CHARMM36 force field and SPC/E water model, and the detailed pipeline can refer to the default workflow of “Free Energy of Solvation”[18]. Energy minimization was conducted utilizing the steepest descent algorithm. To ensure system stability, system equilibration was carried out in two distinct phases (NVT and NPT). Significantly, the temperature parameter in NVT and NPT ensembles should be modified (300 K and 330 K). Molecular docking was performed using Discovery studio 2019, as well as protein sequence alignment.

2.10. Protein crystal structure alignment and data analysis

Structure comparison and alignment were performed by US-align [19] and Discovery studio 2019, and visualized by PyMOL. The variation analysis was performed using R rstatix packages.

2.11. Material characterization experiment by SEM, FTIR, XPS

The specific operation process of scanning electron microscopy (SEM), Fourier transform infra-red (FTIR) spectroscopies FTIR and X-ray photoelectron spectroscopy (XPS) can be referred to this paper[20].

2.12. HPLC analysis of the degradation product of PET

A Waters E2695 chromatographic system, equipped with a HyPURITY C18 column (4.6 × 250 mm), was employed in this study for HPLC analysis. The mobile phase was comprised of a mixture of methanol and 18 mM phosphate buffer, flowing at a rate of 0.5 mL/min, with detection at a wavelength of 240 nm. Elution conditions involved the use of 25% (v/v) methanol for the 0–30 min segment, followed by a 25–100% linear gradient of methanol from 30 to 50 min. The total peak areas of MHET, terephthalic acid (TPA), and bis(2-hydroxyethyl) terephthalate (BHET) were utilized in determining the quantity of product from each PET hydrolysis reaction.

3. Results and discussion

3.1. PET hydrolytic enzymes play a more important role than anchoring proteins

Outer membrane proteins, lipoproteins, fimbria proteins, and flagellar proteins have been widely utilized as effective anchoring proteins in bacterial surface-display construction[21]. However, to our knowledge, few previous studies investigated how the choice of anchor protein affect the activity of the PET hydrolase[22]. Theoretically, the size and structure of target proteins displayed by different anchoring proteins should vary greatly. Therefore, we selected three commonly used but structurally diverse anchor proteins, including pGSA (a kind of Gram-positive bacteria outer membrane protein), inaXN (ice nucleation protein), and estA (outer membrane esterase autotransporter, type 5 secretion systems), and the differences between them can be found in the paper published[23]. We fused ISPETase with above three anchoring proteins to study the effect of anchoring protein on surface-display performance. It is worth noting that two G4S flexible peptides (GGGGSGGGGS)[24] (Fig. 1A) were used to connect the anchoring proteins and target affinity proteins during the construction process, because the absence of flexible peptides could affect the display effect, such as estA. Via the MD simulation, the G4S flexible peptides showed high flexibility, and no binding or entanglement occurred between the anchoring protein and PETase. (Fig. 1D).

PETase can hydrolyze pNPB to p-nitrophenol and butyric acid, which

p-nitrophenol has a strong absorption peak at 405 nm[25]. Under incubation temperatures of 37 °C, 50 °C, and 72 °C, the enzyme activity levels of pGSA-PETase were 3.54%, 3.8%, and 10.8% higher than inaXN-PETase, respectively (Fig. 1B). Similarly, compared to estA-PETase, pGSA-PETase was found little higher under the same incubation temperatures. We surmised that this advantage of pGSA-PETase may be due to the following reasons: 1. smaller interference between the anchor and passenger proteins; 2. codon advantage; 3. shorter length of the fusion protein.

Like the enzyme activity, it was observed that pGSA-PETase exhibited higher PET hydrolysis rates (72 h, 200 mesh) in comparison to inaXN-PETase and estA-pGSA at all tested temperatures. Specifically, the hydrolysis rates of pGSA-PETase were 3.5%, 7.6%, 6.6% and 7.1%, 6.2%, 9.9% higher than inaXN-PETase and estA-pGSA at 37 °C, 50 °C, and 72 °C, respectively (Fig. 1C). However, even with the selection of significantly different anchoring proteins, the variations in hydrolytic capacity among them did not exceed 10%. The strong expression of the target protein driven by the T7 promoter under IPTG induction[26] may potentially mask the differences in the surface-display ability of the target protein to some extent. So, the anchor protein type is not the main consideration on PET hydrolysis by bacterial surface-display. Although the overall improvement is not significant, using pGSA as an anchored protein for PET hydrolyzing in this study was a better choice based on above result. At 50 °C and 72 °C, the bacteria are unable to survive, but it does not affect the activity of the enzyme[27]. This is also one of the advantages of surface-displayed engineered bacteria, as there is no need for cell lysis to release the enzyme. Here, the bacterial cells serve as the biological carriers of the enzyme, and the advantage lies in the rapid proliferation of bacteria. Compared to non-biological materials, it eliminates the need for material synthesis and immobilization processes.

With pGSA as the priority anchoring protein, we systematically investigated four PET hydrolases, including ISPETase, a newly discovered novel carboxylic ester hydrolase PE-H from *P. aestuarii*[28], and two mutants (FAST-PETase[29]:five mutations in ISPETase; LCC-ICCG [9]: four mutations in leaf-branch compost cutinase). We chose the optimal temperatures reported of these enzymes for comparison, and these temperatures were also used in the anchoring protein study above. The enzyme activity of these PET hydrolases varied greatly at different temperatures. At 37 °C, there was an evident peak in the relative enzyme activity of pGSA-PETase (Fig. 1E). Moving onto a slightly higher temperature of 50 °C, pGSA-FAST exhibited the greatest relative enzyme activity. At 72 °C, pGSA-ICCG demonstrated the highest enzyme activity. Overall, the PET hydrolysis enzymes displayed were biologically functional and pGSA-FAST exhibited the highest enzyme activity at 50 °C.

However, relying solely on enzyme activity was insufficient to make a comprehensive comparison of the PET hydrolysis capability of these four surface-displayed *E. coli*. So, we used 4 g PET powder (200 mesh) as the substrate for hydrolysis. Due to slower hydrolysis performance at 37 °C, we extended the reaction time to 72 h, whereas at other temperatures, hydrolysis was still conducted for 24 h. Compared with the un-anchoring FAST-PETase, the pGSA-FAST-PETase surface-displayed bacteria actually improved the hydrolysis rate of PET powder (Fig. 1F). Consistent with the enzyme activity results, pGSA-FAST-PETase showed the highest hydrolysis efficiency for PET powder at 50 °C (24 h), with a weight loss rate of 71.3% (Fig. 1F). Furthermore, both ICCG and FAST-PETase demonstrated superior PET hydrolysis capabilities than ISPETase, in line with the primary objective of FAST-PETase and LCC-ICCG mutation, which aimed to enhance the wild-type enzyme’s thermal stability under high-temperature conditions and then increase its hydrolysis ability. Considering temperature, relative enzyme activity and weight loss rate of PET powder, FAST-PETase is a more optimal choice for PET hydrolysis. Then, we used molecular docking to analyze the binding affinity of the substrate PET3 (three PET molecules polymerized). The results showed that besides common hydrogen bonding, other forces involved included van der Waals forces, hydrophobic

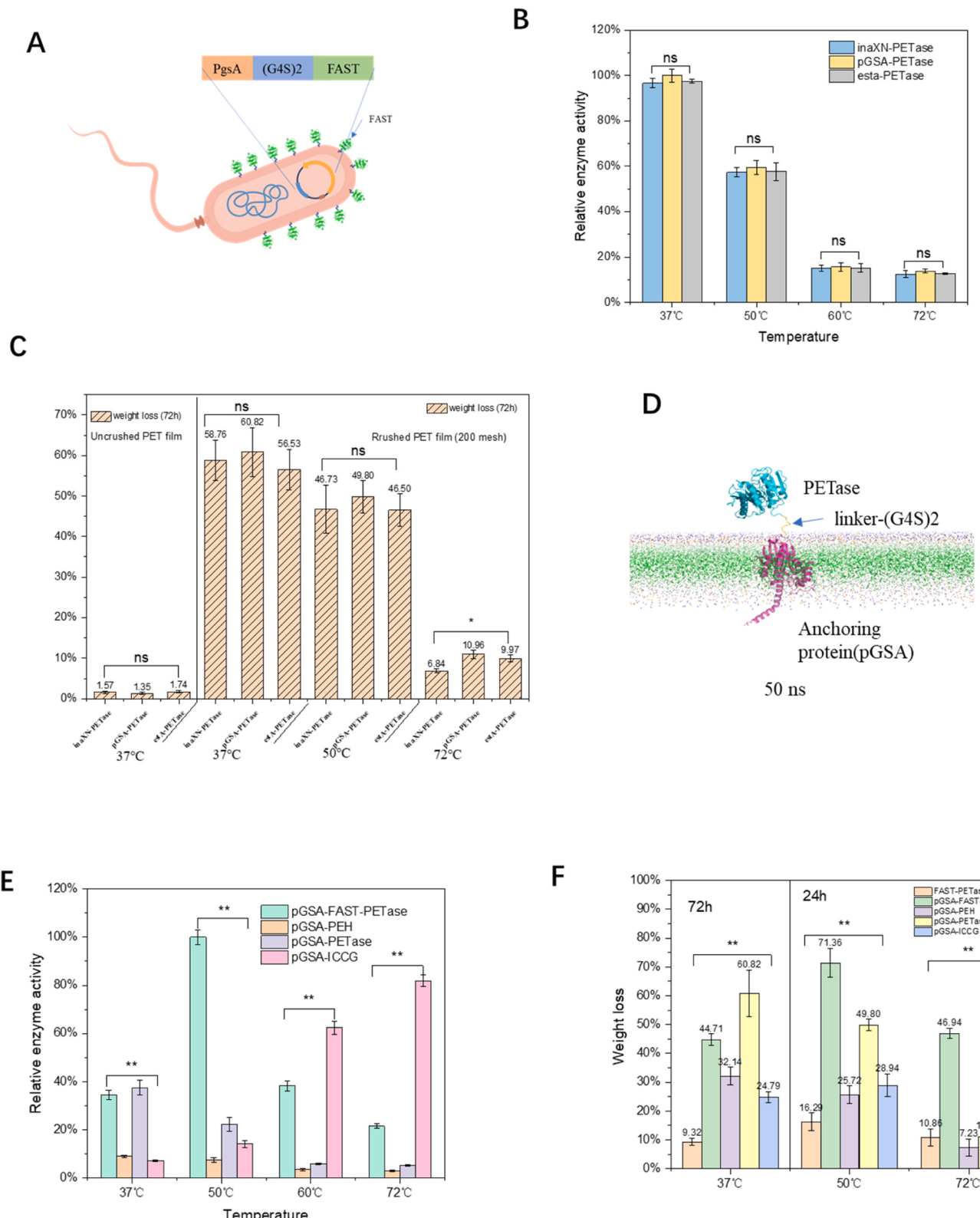


Fig. 1. Anchoring protein selection and surface-display system construction. **A** Schematic diagram of the surface-display system (take pGSA-PETase as an example). **B** Comparison of relative enzyme activity in *E. coli* with different anchoring proteins at different temperature. The highest activity of pGSA-PETase at 37 °C is acted as 100%. **C** The weight loss of PET film and PET film powder by different surface-displayed *E. coli* at three temperatures. **D** MD simulations of the surface-display system over 50 ns. **E** Comparison of relative enzyme activity in surface-displayed engineering *E. coli* with different PET hydrolysis enzyme at different temperature. The highest activity of pGSA-FAST-PETase at 50 °C is acted as 100%. **F** The weight loss of PET film powder by different surface-displayed *E. coli* at three temperatures.

interactions, and various pi bonds (Fig. 2C). This suggests that it is not sufficient to consider only hydrogen bonding when optimizing the binding between substrate and hydrolase, and other forces play a non-negligible role in many cases[30].

Due to the complexity of bacterial membrane structure, proteins surface-displayed on bacterial outer membrane involves complex protein transport and transmembrane processes. Although these anchoring proteins have been demonstrated to be capable of displaying on surface theoretically, reasonable verification is still required for the surface-display of PET hydrolases. Here, three techniques and methods were used to demonstrate the successful display of FAST-PETase on the

surface of *E. coli*. Firstly, we conducted a double-chamber experiment, wherein we placed a 0.22 μm semipermeable membrane between two culture flasks connected to each other (SI Fig. S9). This device prevented the bacterial cells from penetrating the membrane but facilitated the protein molecule transportation, which was similar to the principle of dialysis. After a 72 h hydrolysis, the weight loss rate of PET particles was less than 2% (SI Fig. S13), demonstrating that PET plastics were mainly hydrolyzed by the FAST-PETase on the bacterial outer membrane, and the hydrolysis of PET showed a strong reliance on physical contact to surface-displayed bacteria. Secondly, we used enzyme-linked immunomagnetic bead precipitation, which the His-tagged magnetic bead

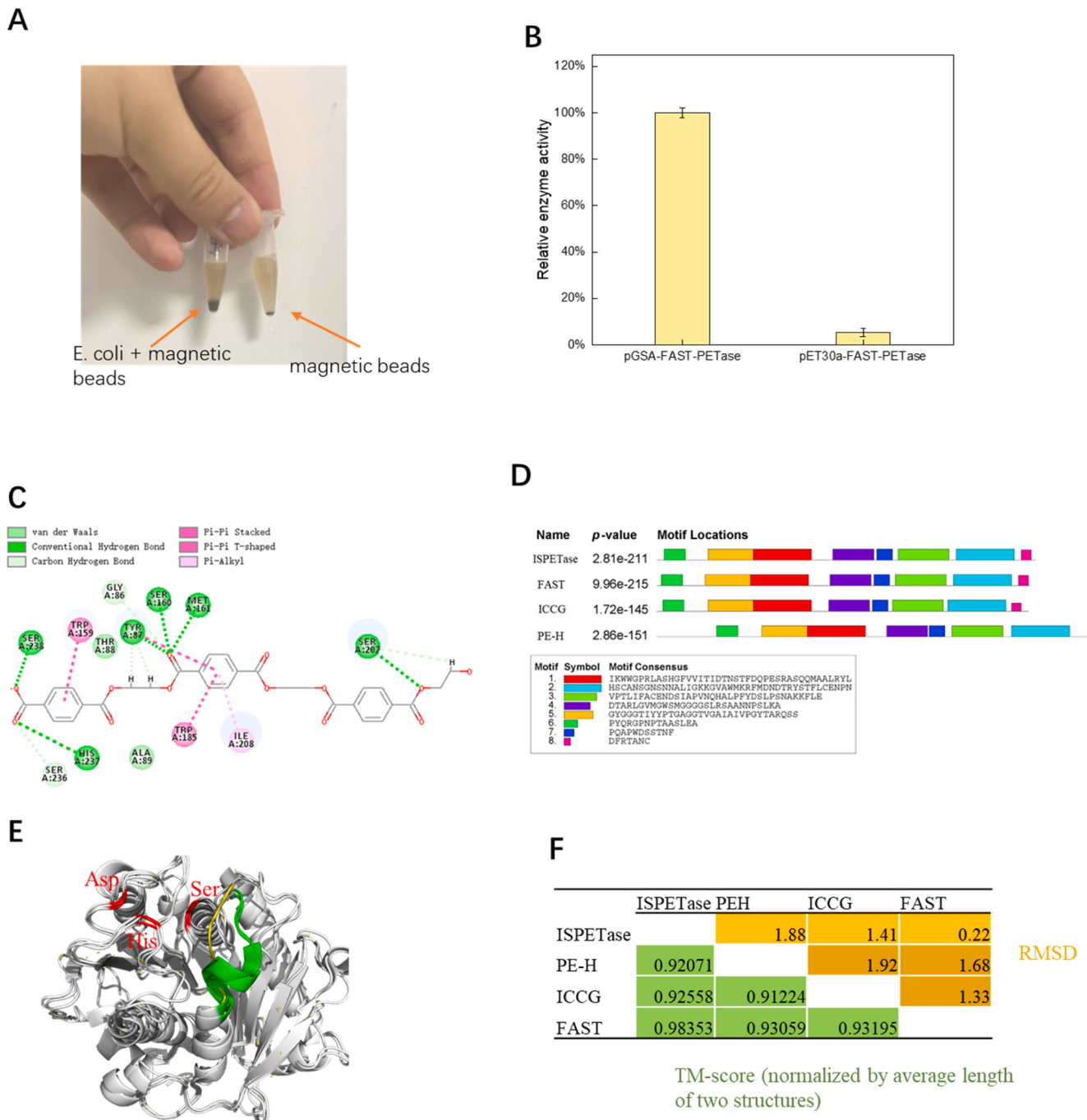


Fig. 2. The proof for FAST-PETase successfully displaying on the surface of *E. coli*. And structure alignment of four PET hydrolysis enzymes. **A** Enzyme-linked immunomagnetic bead precipitation result. **B** The comparison of membrane protein enzyme activity between surface-display by pGSA and un-anchoring FAST-PETase. **C** The interaction force between PET and FAST-PETase by molecular docking result. **D** Protein motif discovery by MEME. **E** Crystal structure superposition of ISPETase, FAST-PETase, ICCG and PE-H. **F** Crystal structure comparison of the four enzymes. Left: TM-score. Right: RMSD.

antibody was employed to bind with the His tag at pGSA-FAST-PETase C-terminal. After magnetic absorption, it was observed that pGSA-FAST-PETase medium became clear but the intracellular expression was not (Fig. 2A). The OD₆₀₀ of surface-displayed bacteria decreased from an initial value of 1.0–0.45, while the intracellular expression bacteria (pET30a-FAST-PETase) remained at around 0.98. Finally, we validated that the hydrolysis activity was mainly exerted by the protein anchored on the outer membrane through extracting the membrane protein of surface-displayed *E. Coli*. Without the pGSA anchoring, the enzyme activity extracted from pET30a-FAST-PETase *E. Coli* membrane protein was substantially lower compared to pGSA-FAST-PETase, accounting for only 5.4% of the latter (Fig. 2B). Based on the above-mentioned three experiments, it can be unequivocally confirmed that FAST-PETase has been successfully anchored onto the outer membrane of the carrier cell.

3.2. The protein structure of PET hydrolases determines their function and stability

In this study, we used the original *ISPETase*, FAST-PETase, PE-H, and a mutant of leaf-branch compost cutinase known as ICCG. Considering the fact that these enzymes have proven their ability to efficiently break down PET, it is logical to assume that they possess certain structural similarities. At first, we aligned the amino acid sequences of these four enzymes and found that although they originated from different microorganisms and enzyme classifications, they shared a relatively high degree of amino acid similarity (~ 50% identity) and possessed the same catalytic triad (the exception of the S160A in ICCG) (SI Fig. S12). PE-H showed the greatest sequence difference from the other three, but even so, it shared more than 45% sequence homology with the PET hydrolases from *S. viridis*, *Thermobifida* sp. and *I. sakaiensis*[28]. Using MEME [31], all these four enzymes possessed the same conserved domains and the conserved domain positions (Fig. 2D). This may imply that the proteins with PET-hydrolyzing capability should exhibit similar or identical structures. However, the primary and secondary structures of proteins alone are not enough to explain their functional similarities and differences. Subsequently, we compared the crystal structures of these four proteins. Through structural overlay analysis, FAST-PETase exhibited an RMSD (root-mean-square deviation) value of just 0.22 Å compared to *ISPETase* (Fig. 2F). In contrast, the RMSD values for ICCG and PE-H (compared to *ISPETase*) were 1.41 Å and 1.88 Å, respectively, conforming well with the findings of the amino acid sequence analysis. Additionally, their structural similarities (TM score) were all greater than 0.9 (Fig. 2F), indicating a very high degree of structural similarity. After superimposing their protein structures, we observed that disparities in structure were predominantly limited to the disordered curves (Fig. 2E), while the alpha helices and beta sheets exhibited striking overlapping, especially for the catalytic triad. These findings suggested that even though these four proteins had the same structure, we may have mislabeled them for different classes. Therefore, we expanded the scope of our protein structure comparison.

We screened 41 enzymes capable of hydrolyzing or degrading PET from the PDB database with available crystal structures, covering almost all of the PET hydrolyzing enzymes (Table 1). Because the structural differences between mutant proteins and their wild-type counterparts were relatively small, we only analyzed the structures of the wild-type proteins and ignored the structural information of the mutants. Based on EC classification and original literature descriptions, the 41 hydrolyzing enzymes were mainly classified into seven categories: *ISPETase* (the benchmark), cutinase, esterase, LCC, PEH (PET hydrolase), TfCut, and potential proteins capable of hydrolyzing PEH, which almost covered all reported PET-degrading enzyme types. USalign[19] (a new structure alignment algorithm) was used to compare the protein structures, with higher TM scores indicating more similar structures. Surprisingly, using *ISPETase* as a benchmark, 36 of the 41 PDB structures had a TM value above 0.9 (Table 1 Structure 1), while the other five structures had much larger differences (TM values below 0.7), which

these five proteins could be further classified into two types according to their similarity. In other words, only three types of protein structures were found from the PET-degrading enzymes, with *ISPETase* as the main representative (Table 1 Structure 1), and the other two types (Table 1 Structure 2 and 3) were significantly different from it with a low proportion. We overlaid these structures and found that the 36 proteins in Structures 1 were almost identical, with the PET-catalytic domain and the main alpha helix and beta-sheet frameworks completely overlapping, and the main differences were only found in the disordered protein curves (Fig. 3A Structure 1). The overlap rates between these 3 structure types were relatively low, and their catalytic structural domains were misaligned (Fig. 3A Structure 1 VS Structure 2 VS Structure 3). Therefore, we question whether we have really discovered new PET-degrading enzymes? Here, we propose three structural types of PET-degrading enzymes: the main type represented by *ISPETase*, the second type represented by *Fusarium oxysporum* cutinase, and the third one represented by *Chloroflexus* sp. MS-G cutinase. Furthermore, it is worth noting that the discovery of TfCut[32] could date back to 2013, pre-dating the more recent discovery of *ISPETase* in 2016. We believe that confusion in naming or classification may have negative affect on the discovery of PET-degrading enzymes, and classification based purely on amino acid sequence or nucleotide sequence similarity perhaps have certain errors. Classifying based on the similarity of protein crystal structure is more scientific and practical.

Enzymes can only function if a stable protein structure is maintained, but as temperatures rising or other conditions changing, proteins will undergo inactivation and deformation, an important aspect of which is the structural changes in proteins, especially backbone changes. Previous studies had shown that protein structural stability was the key to improve PET hydrolysis temperature[9]. Fast-PETase was originally designed to improve the stability of *ISPETase* at high temperatures, as PET tended to be hydrolyzed at higher temperatures. However, the original paper did not perform molecular dynamics simulations, so we aimed to reveal the high-temperature tolerance mechanism of these enzymes from the perspective of protein structural stability using molecular dynamics simulation[33]. We chose two temperatures of 300 K and 330 K for a 50 ns molecular dynamics simulation, which covered the optimal enzymatic activity temperature of these four enzymes (Fig. 3D). The simulation results accorded with the previous experimental data, FAST-PETase and ICCG exhibited better stability in protein backbone at both temperatures with RMSD below 0.15 Å, while *ISPETase*'s stability decreased rapidly at high temperatures with a higher RMSD. Not surprisingly, PEH had the poorest stability (highest RMSD) at both temperatures, which could explain why the hydrolytic activity of PEH decreases the fastest[34]. However, these results cannot explain why the hydrolytic activity of PEH is also lower than PETase at low temperatures. Therefore, we analyzed the protein surface charge interaction potential. ICCG, *ISPETase* and its derivatives FAST-PETase have cracks of about 5 Å at the triple catalytic site, while the catalytic groove of PEH is sealed by electrostatic potential energy (Fig. 3B). Experts believed that this cleft might be very important to accommodate crystalline semi-aromatic polyesters[35] and this may be an intrinsic reason for poor hydrolytic activity of PEH. Additionally, PE-H has the highest self-aggregation tendency via hydrophobic interactions (the lower the DI, the less liable to aggregate) and the least surface charge, in other words, FAST, *ISPETase* and ICCG are more stable than PE-H (Fig. 3C).

The enzymes capable of hydrolyzing PET exhibited similar crystal structures. Therefore, classification of PET-hydrolyzing enzymes should consider their crystal structures, which may facilitate the discovery of novel enzymes. In general, an excellent PET hydrolase should have robust protein skeleton for heat resistance, sufficiently wide catalytic groove to accommodate the PET chain, good affinity to the substrate PET, low self-aggregation tendency (less prone to intertwine between proteins) and reasonable surface charge to ensure its solubility in water, where computer-aided design can play an unexpected role.

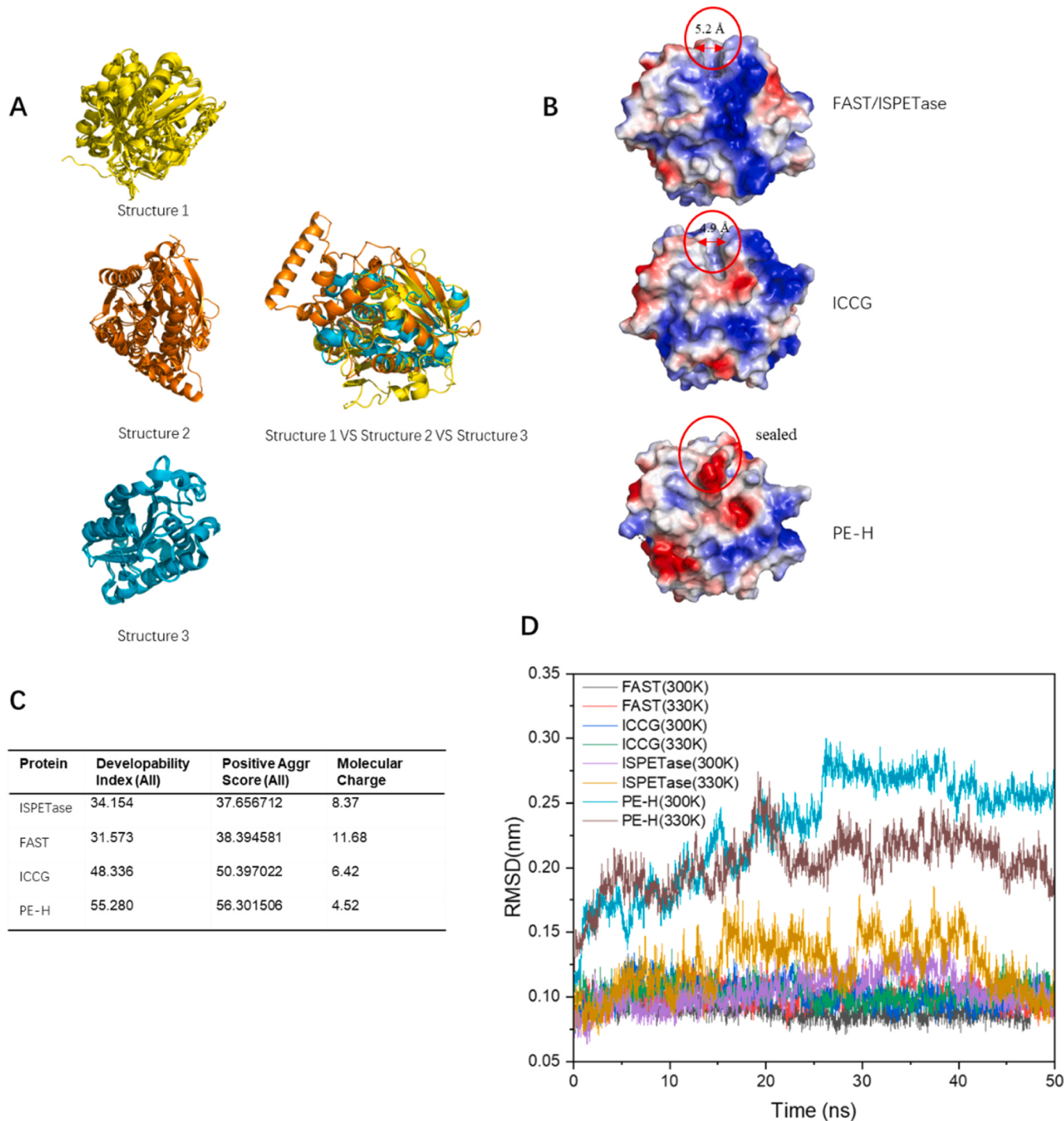


Fig. 3. Crystal structure comparison of PET hydrolysis enzymes and structure stability analyze. A Crystal structure classification and superposition. B There is a clear active-site cleft in ISPETase (FAST) and ICCG crystal structure. C Aggregate propensity analysis. D PE-H and ISPETase show higher RMSD values than ICCG and FAST. Better structural stability corresponds to smaller RMSD values.

3.3. Hydrolysis characteristics of FAST-PETase surface-displayed *E. coli* for PET

Utilizing pNPB as the substrate, FAST-PETase surface-displayed *E. coli* exhibited optimal enzymatic activity at 50 °C (100%). At a higher temperature of 60 °C, the activity of FAST-PETase surface-displayed *E. coli* decreased to only 40% of its maximum activity, while the enzyme maintained a high activity of 71.2% at 42 °C (Fig. 4A). These findings suggest that FAST-PETase needs a specific temperature to exert its maximum hydrolytic activity and high temperature could weaken its

activity quickly. FAST-PETase surface-displayed *E. coli* showed the highest activity at pH 8.5, with more than 80% activity remaining at pH 8 and 9 (Fig. 4B). On the other hand, its hydrolytic activity at pH 6.0 was only 18.3%, which indicated that FAST-PETase surface-displayed *E. coli* was better adapted to alkaline conditions. In practical catalytic reactions, different metal cations might be present in the solution, and they could have certain impacts on the catalytic activity of the enzyme. Under the condition of additional 10 mM ion, we detected that Na⁺, K⁺, and Ca²⁺ could activate FAST-PETase with a maximum activation of 123.2% (Fig. 4C). Previous studies have shown that the addition of

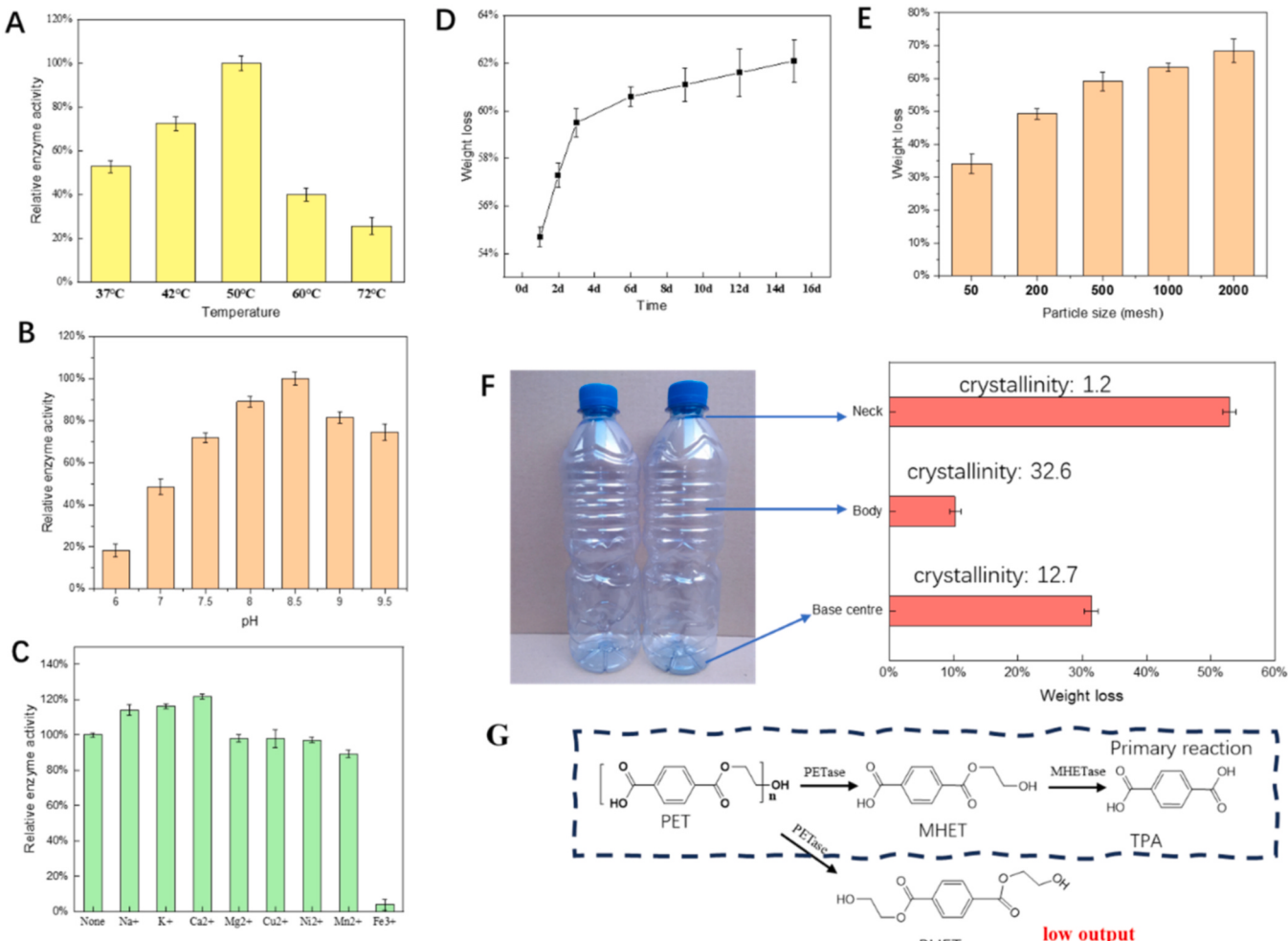


Fig. 4. Enzymatic characteristics and PET hydrolysis characteristics of pGSA-FAST-PETase surface-displayed *E. coli*. **A** The relative enzyme activity of FAST-PETase surface-displayed BL21 at different temperature. **B** The relative enzyme activity of FAST-PETase surface-displayed BL21 at different pH. **C** The effect of metal ions on enzyme activity. **D** Degradation of PET powder with FAST-PETase surface-displayed *E. coli* at 50 °C. **E** Degradation rate of PET powder with different particle size. **F** Depolymerization of top-to-bottom fragments of PET bottle powder by FAST-PETase surface-displayed *E. coli* at 50 °C. **G** Flow chart of the PET hydrolysis products.

calcium ions could enhance the thermal stability of LCC[36], because LCC had an extremely similar structure to FAST-PETase (Table 1), thus it was reasonable to believe that calcium ions could also enhance the stability of other PET hydrolases. Based on our study, K⁺ and Na⁺ ions may have the same effect of Ca²⁺. Although no direct metal-binding sites were identified in the crystal structures of these enzymes, some side-chain amino acids might possess potential for metal binding[9]. By contrast, Mg²⁺, Cu²⁺, and Ni²⁺ had little effect on the enzymatic activity of pGSA-FAST-PETase. Mn²⁺ exhibited a certain inhibitory effect, but its residual activity was still maintained at a level of 89.4%, indicating that pGSA-FAST-PETase had good tolerance to most common metal ions. However, Fe³⁺ almost completely inhibited the activity of pGSA-FAST-PETase (enzyme activity dropped to 3.9%), which may be caused by protein denaturation induced by Fe³⁺.

Using self-purchased amorphous PET powder (200 mesh) as the substrate, we measured the weight loss of PET powder after hydrolysis for 1, 2, 3, 6, 9, 12, and 15 days. As shown in Fig. 4D, after 1 day of hydrolysis by FAST-PETase surface-displayed *E. coli*, the weight loss of PET powder reached to 54.7%. Subsequently, PET hydrolysis became slow, and the hydrolysis rate only reached to 62.1% after 15 days. The hydrolysis rate remained stable from the 3rd day, and this might be directly related to the decrease in enzyme activity and the difficulty of hydrolyzing the PET-resistant part. Although FAST-PETase has improved its hydrolysis ability at high temperatures, future research

should put more effort into how to improve its long-term thermal stability via amino acid mutations. To the best of our knowledge, how to shorten the length of the protein while ensuring the hydrolytic activity of PET may be a solution.

In previous studies, we found that grinding PET plastic could greatly enhance its hydrolysis efficiency. Therefore, we believed that there was a certain relationship between the hydrolysis of PET and its particle size. We measured the weight loss of different sized PET powders (50, 200, 500, 1000, 2000 mesh) using surface-displayed *E. coli* (Fig. 4E). Under the same hydrolysis temperature (50 °C, 24 h), the weight loss of PET powder with 50 mesh was only 34.1%, while it reached around 50% for the PET powder of 200 mesh. As the particle size of PET powder decreased, the hydrolysis rate by pGSA-FAST-PETase increased clearly and the hydrolysis rate of PET powder with 2000 mesh could reach up to 68.4%. The reason may be that PET powder with smaller particle sizes have larger specific surface areas. When hydrolyzed by FAST-PETase surface-displayed *E. coli*, the powder with a larger specific surface area has more chance to contact with bacterial surface, resulting in a higher hydrolysis level[37].

Generally, the hydrolysis of PET is closely related to its crystallinity, with higher crystallinity resulting in poorer hydrolysis efficiency[29]. Unlike plastic products thermoformed, PET water bottles are produced through blow molding, which leads to a high degree of crystallization (>25%) during the expansion process for most bottles[38]. The

crystallinity in the center of the bottle mouth and bottom was relatively low (1.2% and 12.7%, respectively), whereas the crystallinity in the body of the bottle was usually higher (32.6%)^[29]. We cut these regions of PET bottle out, ground them (200 mesh), and treated them with FAST-PETase surface-displayed *E. coli* for 24 h at 50 °C. The results showed that the hydrolysis rate of the bottle neck reached to 52.9%, while the bottle base center was 31.4% (Fig. 4F). However, the hydrolysis rate in the bottle body was only 10.2%. These results indicated that plastic crystallinity could affect the hydrolysis of PET, with higher crystallinity leading to poorer hydrolysis efficiency. It has been proposed that higher temperatures may facilitate the hydrolysis of PET, because PET will undergo glass transition at 70 °C^[39]. However, after careful comparison, it has been established that FAST-PETase exhibits the efficient hydrolysis capacity at 50 °C. This evidence suggested that simply elevating hydrolysis temperature might not be the optimal solution, and a more effective approach would be to design enzymes with appropriate structural characteristics.

3.4. The change of PET surface morphology and properties after hydrolysis

By surface-displayed *E. coli* hydrolysis, the main products of PET were MHET, TPA, and BHET (SI Fig. S14 A). MHET is the main product in the first step of PET hydrolysis and will be further hydrolyzed to TPA, while BHET is the by-product (Fig. 4G). Because BHET is solely found at the end of hydrolyzed polymer chains, its production yield is limited [14]. From a comprehensive view of the reaction process, equilibrium was reached at approximately 21 h after hydrolysis initiation, and the accumulation amount of MHET stabilized at around 18 h. Combined with the enzymatic activity findings, the reduced hydrolysis of PET could be attributed to two factors: a decline in enzyme activity, as well as a possible decrease in mass transfer rate that due to product accumulation. After 24 h of hydrolysis by FAST-PETase surface-displayed *E. coli*, 250 mg PET powder produced about 8.5 mM MHET and 1.6 mM TPA (Fig. 5A), which FAST-PETase exhibited some ability to hydrolyze MHET to TPA.

In order to obtain more intuitive evidence, we studied the changes of PET plastic after hydrolysis. SEM directly observed the morphological changes of PET plastics, which proved the hydrolysis and erosion of PET plastics by surface-displayed bacteria. SEM images of PET powder taken before hydrolysis showed a relatively smooth surface, while the surface became rough and pocked with numerous small pores after the hydrolysis of surface engineered *E. coli* (Fig. 5B). After hydrolysis, the PET powder became very fragmented, as a result, decreased in weight.

FTIR is a valuable technique for monitoring the chemical bond cleavage and formation of functional groups in PET molecular chains. Further analysis using FTIR indicated that hydrolysis promoted the oxidation of PET materials, resulting in a significant increase of oxygen-containing groups, with the most typical example being the more pronounced peak in the C=O absorption peak at 1713 cm⁻¹ (Fig. 5C). Moreover, as the reaction proceeding, the relative intensity of the freestanding hydroxyl group at 3540 cm⁻¹ weakened, indicating further oxidation of hydroxyl structures into acid and ester compounds might occur. These results are consistent with subsequent XPS analysis.

By observing the changes in the C1s and O1s spectral peaks of XPS, the types of surface functional groups in PET can be determined. In XPS analysis, the C1s spectrum and O1s spectrum primarily reflects the chemical state and presence of carbon elements and oxygen elements, respectively, and the difference of PET hydrolysis was mainly in O1s. The peaks of high-resolution XPS-O1s spectra at 531.73 eV and 533.34 eV could be attributed to C=O and C-O, which represented the ester groups in PET. After hydrolysis of PET, the relative content of C=O increased from 52.89% to 63.60%, while the relative content of C-O became 36.4% (Fig. 5D), which showed that surface-displayed engineered bacteria participated in the oxidation of PET plastic and changed PET surface functional groups. We believe this is due to the hydrolysis of

PET plastic, where more long chains are hydrolyzed into short chains, exposing carbonyl end groups. Additionally, combined with the results of SEM analysis, the surface of PET plastic becomes rough, leading to an increase in the proportion of carbonyl end groups.

3.5. The recombinant proteins C-terminal has an effect on PET hydrolysis

The main hydrolysis product of PET by FAST-PETase is MHET, and complete hydrolysis requires cooperative action between PETase and MHETase. Thus, we planned to co-display both MHETase and FAST-PETase through flexible peptide linkages (G4S), co-anchoring them in the outer membrane of *E. coli* (Fig. 5E). Since the two-enzyme system involved the question of which enzyme was more suitable at the C-terminal (N-terminal is inside the membrane, C-terminal is outside), so the effect of the recombinant protein C-terminal region on PET hydrolysis was assessed. Regardless of which enzyme was located at the C-terminal, the two-enzyme system showed enhanced PET hydrolysis performance (Fig. 5F and Fig. 4D), suggesting that MHETase could break the hydrolysis decline caused by substrate MHET accumulation. Interestingly, the PET hydrolytic rate of the C-terminal pGSA-MHETase-g4s-FAST-PETase (84.6%) was slightly higher than the N-terminal one (pGSA-FAST-PETase-g4s-MHETase, 80.8%) after 24 h (Fig. 5F). Given that enzyme contact was essential for the hydrolysis of PET, the C-terminal end of recombinant protein offered a distinct advantage. And it also confirmed our previous hypothesis that substrate accumulation could affect the hydrolysis ability. Although it had been shown that MHETase and PETase could improve the hydrolysis efficiency of PET by cooperating with each other^[40], our study provided a new idea to achieve the coexistence of the two enzymes by the mean of surface co-display. It is worth mentioning that it has been found that MHETase has an exo-PETase activity, allowing hydrolysis PET at the terminal ester groups^[41], which further enhanced the hydrolysis ability.

In addition to the difference in hydrolysis capacity, whether the hydrolyzed products are also different. So, we examined whether the hydrolysis products of the two recombinant proteins differed in PET hydrolysis (250 mg). Like the FAST-PETase surface-display system, both co-display fusion proteins generated MHET, TPA and BHET (SI Fig. S14 B). However, there was a significant difference in the production of TPA and MHET between the two recombinant proteins. Specifically, C terminal pGSA-MHETase-g4s-FAST-PETase yielded less TPA (6.9 mM TPA, 4.2 mM MHET) (Fig. 5G). By contrast, pGSA-FAST-PETase-g4s-MHETase produced higher ratio of TPA (7.0 TPA mM and 3.3 mM MHET) (Fig. 5H). These results indicated that the C-terminal of the fused protein was the most favorable position, where FAST-PETase located at the C-terminal could lead to a higher degree of PET hydrolysis, while MEHTase located at the C-terminal resulted in more MHET hydrolysis. To gain more insight, it would be useful to explore the structural changes or conformational dynamics of fusion proteins when they are at different ends, and AlphaFold2 is helpful to gain the fusion proteins^[42]. However, in general, for faster PET hydrolysis, FAST-PETase is more suitable at the C-terminal of co-display system.

CRediT authorship contribution statement

Ying Zhang: Writing – review & editing (equal). **Wei Han:** Conceptualization (lead), Writing (lead). **Jun Zhang:** Methodology (lead). **Qi Chen:** Software (lead). **Yuzhu Xie:** Software (equal). **Meng Zhang:** Writing (equal). **Jianhua Qu:** Visualization (equal). **Yuanji Tan:** Visualization (equal). **Yiran Diao:** Visualization (equal).

Environmental Implication

Polyethylene terephthalate (PET) is one of the most widely used plastics, and it has caused some adverse effects in the environment. We comprehensively compared several newly reported PET hydrolases, and rationally designed the optimal surface-displayed engineering bacteria,

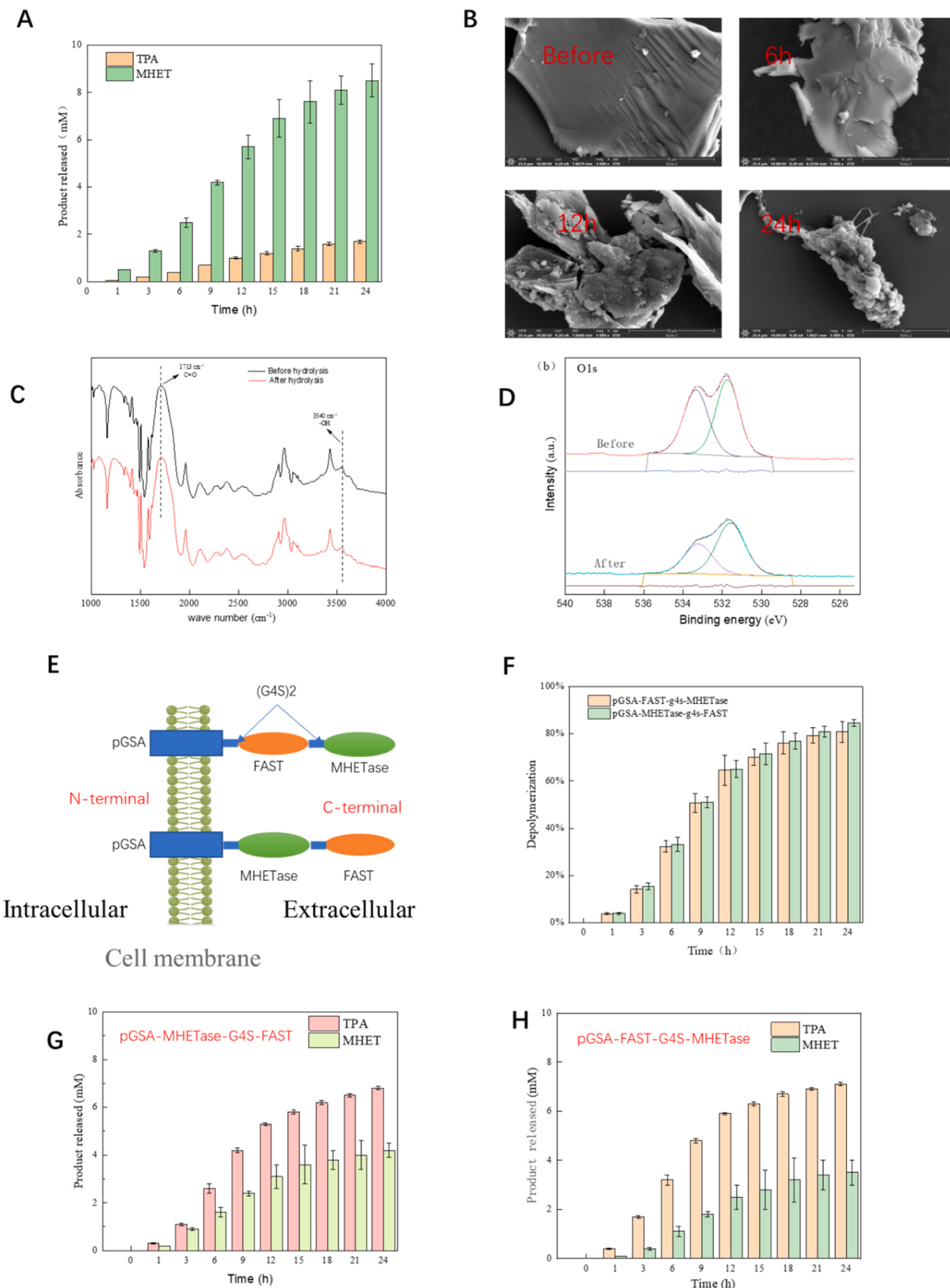


Fig. 5. PET surface morphology and property change and MHETase-FAST co-surface display system construction. **A** The changes in products during PET hydrolysis. **B** PET powder surface morphology by SEM. **C** FTIR result. **D** XPS spectrum comparison. **E** Schematic diagram of the co-display system of MHETase and FAST-PETase. **F** FAST-PETase is more advantageous at C terminal. **G** and **H** The changes in products during PET hydrolysis by two different co-display build strategies.

the results show that it has a good hydrolysis effect on PET plastics.

Declaration of Competing Interest

The authors declare that they have no known competing financial interests or personal relationships that could have appeared to influence the work reported in this paper.

Data Availability

The data that has been used is confidential.

Acknowledgements

This work was supported by the National Natural Science Foundation of China [grant numbers 32101362]; The Natural Science Foundation of Heilongjiang Province [grant numbers LH2022D005]; Heilongjiang Provincial Key Laboratory of Soil Protection and Remediation.

Appendix A. Supporting information

Supplementary data associated with this article can be found in the online version at doi:10.1016/j.jhazmat.2023.132632.

References

- [1] Mudondo, J., Lee, H.S., Jeong, Y., Kim, T.H., Kim, S., Sung, B.H., Park, S.H., Park, K., Cha, H.G., Yeon, Y.J., Kim, H.T., 2023. Recent advances in the chemobiological upcycling of polyethylene terephthalate (PET) into value-added chemicals. *J Microbiol Biotechnol* 33, 1–14.
- [2] Cusano, I., Campagnolo, L., Aurilia, M., Costanzo, S., Grizzuti, N., 2023. Rheology of recycled PET. *Mater* (Basel, Switz) 16.
- [3] You, Y., Thrush, S.F., Hope, J.A., 2020. The impacts of polyethylene terephthalate microplastics (mPETs) on ecosystem functionality in marine sediment. *Mar Pollut Bull* 160.
- [4] M.S. Bhuyan, S. Venkatraman, S. Selvam, S. Szabo, M.M. Hossain, M. Rashed-Un-Nabi, C.R. Paramasivam, M.P. Jonathan, M.S. Islam, Plastics in marine ecosystem: A review of their sources and pollution conduits (vol 41, 101539, 2021), *Regional Studies in Marine Science*, 44 (2021).
- [5] Chen, C.-C., Han, X., Ko, T.-P., Liu, W., Guo, R.-T., 2018. Structural studies reveal the molecular mechanism of PETase. *FEBS J* 285, 3717–3723.
- [6] Yoshida, S., Hiraga, K., Takehana, T., Taniguchi, I., Yamaji, H., Maeda, Y., Toyohara, K., Miyamoto, K., Kimura, Y., Oda, K., 2016. A bacterium that degrades and assimilates poly(ethylene terephthalate). *Science* 351, 1196–1199.
- [7] Tamoor, M., Samak, N.A., Jia, Y., Mushtaq, M.U., Sher, H., Bibi, M., Xing, J., 2021. Potential use of microbial enzymes for the conversion of plastic waste into value-added products: a viable solution. *Front Microbiol* 12, 777727.
- [8] Lu, H., Diaz, D.J., Czarnecki, N.J., Zhu, C., Kim, W., Shroff, R., Acosta, D.J., Alexander, B.R., Cole, H.O., Zhang, Y., Lynd, N.A., Ellington, A.D., Alper, H.S., 2022. Machine learning-aided engineering of hydrolases for PET depolymerization. *Nature* 604, 662.
- [9] Tournier, V., Topham, C.M., Gilles, A., David, B., Folgoas, C., Moya-Leclair, E., Kamionka, E., Desrousseaux, M.L., Texier, H., Gavalda, S., Cot, M., Guémaré, E., Dalibey, M., Nomme, J., Cioci, G., Barbe, S., Chateau, M., André, I., Duquesne, S., Marty, A., 2020. An engineered PET depolymerase to break down and recycle plastic bottles. *Nature* 580, 216–219.
- [10] Pham, M.L., Polaković, M., 2020. Microbial cell surface display of oxidoreductases: concepts and applications. *Int J Biol Macromol* 165, 835–841.
- [11] Zhang, C., Chen, H., Zhu, Y., Zhang, Y., Li, X., Wang, F., 2022. *Saccharomyces cerevisiae* cell surface display technology: Strategies for improvement and applications. *Front Bioeng Biotechnol* 10, 1056804.
- [12] Heyde, S.A.H., Arnling Bååth, J., Westh, P., Nørholm, M.H.H., Jensen, K., 2021. Surface display as a functional screening platform for detecting enzymes active on PET. *Microb Cell Factor* 20, 93.
- [13] Loll-Krippleber, R., Sajtovich, V.A., Ferguson, M.W., Ho, B., Burns, A.R., Payliss, B., Bellissimo, J., Peters, S., Roy, P.J., Wyatt, H.D.M., Brown, G.W., 2022. Development of a yeast whole-cell biocatalyst for MHET conversion into terephthalic acid and ethylene glycol. *Microb Cell Factor* 21, 280.
- [14] Chen, Z., Wang, Y., Cheng, Y., Wang, X., Tong, S., Yang, H., Wang, Z., 2020. Efficient biodegradation of highly crystallized polyethylene terephthalate through cell surface display of bacterial PETase. *Sci Total Environ* 709, 136138.
- [15] Hou, X.-L., Yu, L.-Y., Liu, J., Wang, G.-H., 2007. Surface-displayed porcine epidemic diarrhea viral (PEDV) antigens on lactic acid bacteria. *Vaccine* 26, 24–31.
- [16] He, X., Chen, W., Huang, Q., 2012. Surface display of monkey metallothionein α tandem repeats and EGFP fusion protein on *Pseudomonas putida* X4 for biosorption and detection of cadmium. *Appl Microbiol Biotechnol* 95, 1605–1613.
- [17] Yang, T.H., Pan, J.G., Seo, Y.S., Rhee, J.S., 2004. Use of *Pseudomonas putida* EstA as an anchoring motif for display of a periplasmic enzyme on the surface of *Escherichia coli*. *Appl Environ Microbiol* 70, 6968–6976.
- [18] J. Lemkul, From Proteins to Perturbed Hamiltonians: A Suite of Tutorials for the GROMACS-2018 Molecular Simulation Package [Article v1.0], (2018).
- [19] Zhang, C., Shine, M., Pyle, A.M., Zhang, Y., 2022. US-align: universal structure alignments of proteins, nucleic acids, and macromolecular complexes. *Nat Methods* 19, 1109–1115.
- [20] Parmanbek, N., Sütekin, S.D., Barsbay, M., Aimanova, N.A., Mashentseva, A.A., Alimkhanova, A.N., Zhumabayev, A.M., Yanovich, A., Almanov, A.A., Zdrovovets, M.V., 2023. Environmentally friendly loading of palladium nanoparticles on nanoporous PET track-etched membranes grafted by poly(1-vinyl-2-pyrrolidone) via RAFT polymerization for the photocatalytic degradation of metronidazole. *RSC Adv* 13, 18700–18714.
- [21] M. Park, Surface Display Technology for Biosensor Applications: A Review, *Sensors* (Basel, Switzerland), 20 (2020).
- [22] Gao, R., Pan, H., Lian, J., 2021. Recent advances in the discovery, characterization, and engineering of poly(ethylene terephthalate) (PET) hydrolases. *Enzym Microb Technol* 150, 109868.
- [23] van Bloois, E., Winter, R.T., Kolmar, H., Fraaije, M.W., 2011. Decorating microbes: surface display of proteins on *Escherichia coli*. *Trends Biotechnol* 29, 79–86.
- [24] Chen, X., Zaro, J.L., Shen, W.C., 2013. Fusion protein linkers: property, design and functionality. *Adv Drug Deliv Rev* 65, 1357–1369.
- [25] Furukawa, M., Kawakami, N., Tomizawa, A., Miyamoto, K., 2019. Efficient degradation of poly(ethylene terephthalate) with *thermobifida fusca* cutinase exhibiting improved catalytic activity generated using mutagenesis and additive-based approaches. *Sci Rep* 9, 16038.
- [26] Wagner, S., Baars, L., Ytterberg, A.J., Klussmeier, A., Wagner, C.S., Nord, O., Nygren, P.A., van Wijk, K.J., de Gier, J.W., 2007. Consequences of membrane protein overexpression in *Escherichia coli*. *Mol Cell Prote: MCP* 6, 1527–1550.
- [27] Fang, Y., Chao, K., He, J., Wang, Z., Chen, Z., 2023. High-efficiency depolymerization/degradation of polyethylene terephthalate plastic by a whole-cell biocatalyst. *3 Biotech* 13, 138.
- [28] Bollinger, A., Thies, S., Knieps-Grünhagen, E., Gertzen, C., Kobus, S., Höppner, A., Ferrer, M., Gohlke, H., Smits, S.H.J., Jaeger, K.E., 2020. A novel polyester hydrolase from the marine bacterium *pseudomonas aestusnigri* - structural and functional insights. *Front Microbiol* 11, 114.
- [29] Lu, H., Diaz, D.J., Czarnecki, N.J., Zhu, C., Kim, W., Shroff, R., Acosta, D.J., Alexander, B.R., Cole, H.O., Zhang, Y., Lynd, N.A., Ellington, A.D., Alper, H.S., 2022. Machine learning-aided engineering of hydrolases for PET depolymerization. *Nature* 604, 662–667.
- [30] Gao, S., Li, Q., Zhang, S., Sun, X., Zhou, H., Wang, Z., Wu, J., 2023. A novel biosensing platform for detection of glaucoma biomarker GDF15 via an integrated BLI-ELASA strategy. *Biomaterials* 294, 121997.
- [31] Bailey, T.L., Johnson, J., Grant, C.E., Noble, W.S., 2015. The MEME suite. *Nucleic Acids Res* 43, W39–W49.
- [32] Roth, C., Wei, R., Oeser, T., Then, J., Föllner, C., Zimmermann, W., Sträter, N., 2014. Structural and functional studies on a thermostable polyethylene terephthalate degrading hydrolase from *Thermobifida fusca*. *Appl Microbiol Biotechnol* 98, 7815–7823.
- [33] Huang, Z., Ni, D., Chen, Z., Zhu, Y., Zhang, W., Mu, W., 2023. Application of molecular dynamics simulation in the field of food enzymes: improving the thermal-stability and catalytic ability. *Crit Rev Food Sci Nutr* 1–13.
- [34] Patil, S.B., Gadad, P.C., 2023. Elucidation of intermolecular interactions between chlorogenic acid and glucose-6-phosphate translocase: a step towards chemically induced glycogen storage disease type 1b model. *3 Biotech* 13, 250.
- [35] Austin, H.P., Allen, M.D., Donohoe, B.S., Rorrer, N.A., Kearns, F.L., Silveira, R.L., Pollard, B.C., Dominick, G., Duman, R., El Omari, K., Mykhaylyk, V., Wagner, A., Michener, W.E., Amore, A., Skaf, M.S., Crowley, M.F., Thorne, A.W., Johnson, C. W., Woodcock, H.L., McGeehan, J.E., Beckham, G.T., 2018. Characterization and engineering of a plastic-degrading aromatic polyesterase. *Proc Natl Acad Sci USA* 115, E4350–e4357.
- [36] Sulaiman, S., You, D.J., Kanaya, E., Koga, Y., Kanaya, S., 2014. Crystal structure and thermodynamic and kinetic stability of metagenome-derived LC-cutinase. *Biochemistry* 53, 1858–1869.
- [37] Zhao, J., Lin, M., Chen, G., 2018. Facile recycling of *Escherichia coli* and *Saccharomyces cerevisiae* cells from suspensions using magnetic modification method and mechanism analysis. *Coll. Surf. B Biointerfaces* 169, 1–9.
- [38] M. Kutz, Applied Plastics Engineering Handbook: Processing, Materials, and Applications: Second Edition, (2016).
- [39] Wei, R., Zimmermann, W., 2017. Microbial enzymes for the recycling of recalcitrant petroleum-based plastics: how far are we? *Microb Biotechnol* 10, 1308–1322.
- [40] Qi, X., Ma, Y., Chang, H., Li, B., Ding, M., Yuan, Y., 2021. Evaluation of PET degradation using artificial microbial consortia. *Front Microbiol* 12, 778828.
- [41] Sagong, H.-Y., Seo, H., Kim, T., Son, H.F., Joo, S., Lee, S.H., Kim, S., Woo, J.-S., Hwang, S.Y., Kim, K.-J., 2020. Decomposition of the PET film by MHETase using Exo-PETase function. *ACS Catal* 10, 4805–4812.
- [42] Qiu, Y., Wei, G.W., 2023. Artificial Intelligence-aided Protein Engineering: from Topological Data Analysis to Deep Protein Language Models. *ArXiv*.